Efficient and Robust Approaches to the Stability Analysis of Large Multibody Systems

Olivier A. Bauchau and Jielong Wang

Daniel Guggenheim School of Aerospace Engineering,
Georgia Institute of Technology, 270 Ferst Dr.,
Atlanta, GA 30332, USA
Email: olivier.bauchau@ae.gatech.edu, gtg136j@prism.gatech.edu

Abstract

Linearized stability analysis methodologies that are applicable to large scale, multi-physics problems are presented in this paper. Two classes of closely related algorithms based on a partial Floquet and on an autoregressive approach, respectively, are presented in common framework that underlines their similarity and their relationship to other methods. The robustness of the proposed approach is improved by using optimized signals that are derived from the proper orthogonal modes of the system. Finally, a signal synthesis procedure based on the identified frequencies and damping rates is shown to be an important tool for assessing the accuracy of the identified parameters; furthermore, it provides a means of resolving the frequency indeterminacy associated with the eigenvalues of the transition matrix for periodic systems. The proposed approaches are computationally inexpensive and consist of purely post processing steps that can be used with any multi-physics computational tool or with experimental data. Unlike classical stability analysis methodologies, it does not required the linearization of the equations of motion of the system.

Key words: Multibody systems, Stability analysis, Partial Floquet method, Autoregressive method

1 Introduction

An important aspect of the dynamic response of flexible multi-body systems is the potential presence of instabilities. The instability of a cantilevered beam subjected to a tip, compressive follower force [1], or the instabilities appearing in rotor [1] dynamics [2,3] are but

[1] *Journal of Computational and Nonlinear Dynamics*, **3**(1), pp 011001-1 12, 2008

two well-known types instabilities that can occur in dynamical systems and flexible multibody systems. If the equations of motion of the system can be cast in the form of linear, ordinary differential equations with constant coefficients, classical stability analysis methodologies based on the characteristic exponents of the system can be used. On the other hand, when the equations of motion of the system are cast in the form of linear, ordinary differential equations with periodic coefficients, Floquet's theory [4,5] is used. Stability analysis is typically performed on simplified models with the smallest number of degrees of freedom required to capture the physical phenomenon that causes the instability. As the number of degrees of freedom used to represent the system increases, these methods become increasingly cumbersome, and quickly unmanageable.

Due to increased available computer power, the analysis of flexible multibody systems relies on increasingly complex, large scale models. Full finite element analysis codes are now routinely used for this purpose [6,7,8] and, more often than not, multibody models are coupled to other codes to capture multi-physics phenomena. For instance, the analysis of the ride quality of a road vehicle might require the coupling of a multibody representation of the suspension system to an engine model. For aeroelastic problems, the structural dynamics model of the flight vehicle must be coupled to fluid dynamics code that predicts the aerodynamic forces acting on the structure.

Bauchau and Wang [9], have reviewed several approaches to stability analysis and their applicability to large scale multibody system. They point out that the only approach that gives information about *nonlinear stability* is Lyapunov's function method, which can clearly not be applied to large dimensional numerical models. Hence, the problem of linearized stability is addressed in this paper, *i.e* the stability of small perturbations about a nonlinear equilibrium configuration that could be periodic. For large multibody models, a formal linearization is difficult and costly to obtain for constant in time systems, and virtually impossible in the case of periodic systems. This is particularly true when multi-physics models are coupled to multibody simulations. Hence, the only option is to study the response of the system to small perturbations about an equilibrium configuration using a fully nonlinear, coupled simulation tool. This means, in effect, that the complex dynamic model is used as a virtual prototype of the actual dynamical system, and the analyst is running a set of "experiments" to determine the stability characteristics of the system. A similar approach was taken by other researchers [10,11,12,13] for systems modeled by simple analytical models featuring a few degrees of freedom.

In this framework, the actual sensors that experimentally measure the response of a physical system are replaced by "sensors" that extract from the numerical model the predicted response of the system. In an experimental setting, the number of available sensors is typically limited because the complexity and cost of the experiment will dramatically increase with the number of sensor. Hence, the location and nature of the sensors will be carefully selected so as to obtain high quality measurements that are most relevant to the phenomenon under scrutiny. On the other hand, in a numerical setting, the very nature of computational simulations implies that the response of each degree of freedom is available at no additional cost. The analyst could select a small number of these signals to perform stability analysis,

mimicking the process used in an experimental setting, but it is also possible to use all the available data in an effort to obtain more accurate predictions.

In an experimental setting, stability analysis methods must be robust enough to deal with experimental noise. Numerical implementation also involves noise associated with the time discretization and inaccuracies of the solution. Another source of noise is the fact that the computed response is not that of a linear system, but rather that of a nonlinear system acted upon by small perturbations. In practice, this is a major hurdle: if the perturbation is too large, the nonlinearity in the response is pronounced and linearized stability tools give erroneous stability characteristics; on the other hand, if the perturbation is too small, the response has a small amplitude that becomes indistinguishable from the numerical noise, leading once again to erroneous predictions. If all the predictions produced by the numerical simulation are used for stability analysis, the data set will be highly redundant: the important information is a small subset of the large, noisy, highly redundant data set. This discussion clearly indicates that noise is as much a problem for numerical methods as it is for experimental methods.

In this paper, two algorithms are presented for stability analysis based on techniques that are widely used in system identification, model reduction, linear control, and signal processing. In broad terms, these methods [14] are based on two techniques: the singular value decomposition and polynomial or moment matching concepts. The first type of algorithms are directly derived from linear time-invariant state space models. The relationship between the impulse response of the system at two consecutive time steps leads to the classical Ho and Kalman's algorithm [15]; subsequently, this approach was modified to yield the eigensystem realization algorithm [16] that involves the singular value decomposition. A variant of these approaches, first derived by Moore [17], is known as the balanced truncation method, and additional modifications of the approach are found in ref. [18]. The polynomial based methods are generated from autoregressive moving average models [19], an approach which is equivalent to that used for linear, time-invariant state space models. When impulse responses are solely considered, the autoregressive moving average model reduces to the autoregressive formulation. Bauchau and Wang [9] have proved that Prony's method is, in effect, an autoregressive method, although it is often presented as a curve fitting procedure.

To eliminate the effect of noise in the measured signals, numerous modifications of autoregressive methods has been developed [20,21]. A widely used approach to noise filtering is based on the singular values truncation technique. It has been proved that singular value decomposition associated with Hankel-norm model reduction [22], is equivalent to finite impulse response filtering [23]. The proper orthogonal decomposition [24], often performed via singular value decomposition, is also an efficient noise filtering technique that has been widely applied to fluid problems [25]; it also forms the basis for model reduction techniques in solid mechanics [26] and nonlinear control [27]. The physical interpretation of the proper orthogonal modes is discussed in refs. [28,29]

The two algorithms presented in this paper are closely related to the above two classes of methods and since stability is the focus of the present work, they will be introduced through

Floquet's theory for the first and autoregressive concepts for the second. Since the singular value decomposition is such a powerful tool to deal with noise, both approaches make use of this technique. The proposed algorithms can be applied to one or multiple time signals, and are able to deal with time constant or periodic systems. The algorithms are equally applicable to experimental measurements or numerically computed responses. If all signals are used, *i.e.* if the time histories of all the degrees of freedom of the system are used, the computational burden associated with these algorithms becomes large. One option is to retain a few signals only to reduce the computational cost, but at the expense of loosing potentially relevant information contained in the discarded signals. In this paper, a different approach is taken. First, the proper orthogonal decomposition technique is applied to the full set of all degrees of freedom. The few proper orthogonal modes associated with the largest amount of energy contained in the responses of all degrees of freedom are retained and used as an input to the stability analysis algorithms. This approach is computationally efficient, while retaining accuracy and requiring minimum user input.

2 Model of the system

The systems to be investigated here are assumed to be linear models featuring constant or periodic coefficients. In first order form, the governing equations are written as

$$\dot{\underline{u}}(t) = A\underline{u}(t) + \underline{f}(t), \tag{1}$$

where $\underline{u}(t)$ is the state vector of dimension $2N$, A the system characteristic matrix, and $\underline{f}(t)$ is related to the externally applied forces; the notation $()^{\cdot}$ indicates a derivative with respect to time. Eq. (1) could represent the first order form of the equations of motion of a multibody system, in which case the state vector would store the displacements and velocities of all degrees of freedom of the model. For multi-physics models, the state vector would include additional information; for instance, fluid pressures and velocities in the case of an aeroelastic simulation. It is well known that the stability characteristics of the system properties are determined by the characteristic matrix of the system; hence, in the present work, the sole homogeneous problem is considered

$$\dot{\underline{u}}(t) = A\underline{u}(t). \tag{2}$$

At first, consider a system featuring constant coefficients, *i.e.* A is a constant matrix. Given initial conditions, $\underline{u} = \underline{u}_0$ at time t_0, the solution of the system is given in textbooks [4] as

$$\underline{u}(t) = e^{A(t-t_0)}\underline{u}_0. \tag{3}$$

In numerical applications, the response of the system will typically be computed at a set of discrete times $t_k = k\Delta t$, where Δt is the time step and k a positive integer. Without loss of generality, the initial time can be assumed to be zero, *i.e.*, $t_0 = 0$. The discrete solution at time t_k now writes $\underline{u}(t_k) = \underline{u}_k = \exp(Ak\Delta t)\ \underline{u}_0$, and at time step $k+1$, it is clear that

$\underline{u}_{k+1} = \exp(A\Delta t)\ \underline{u}_k$. The discrete time model can now be written in a compact form as

$$\underline{u}_{k+1} = A_s \underline{u}_k, \quad A_s = \exp(A\Delta t). \tag{4}$$

Next, consider a system with periodic coefficients, *i.e.* matrix A is a periodic function of time, $A(t) = A(t+T)$, where T is the period of the system. Here again, the solution of the problem is found in textbooks [4], and given a set of initial conditions, the solution becomes

$$\underline{u}(t) = P(t) e^{\Lambda(t-t_0)} P^{-1}(t_0) \underline{u}_0; \tag{5}$$

where $\Lambda = \mathrm{diag}(\lambda_i)$ is a diagonal matrix of characteristic exponents of the periodic system and $P(t)$ a periodic matrix, $P(t) = P(t+T)$. The discrete solution now becomes $\underline{u}_k = P_k \exp(\Lambda k \Delta t) P_0^{-1} \underline{u}_0$. Finally, the discrete time model is recast in a compact form as

$$\underline{u}_{k+1} = A_k \underline{u}_k, \quad A_k = P_{k+1} e^{\Lambda \Delta t} P_k^{-1}. \tag{6}$$

Because the system is periodic, it follows that $A_k = A_{k+p}$, where p is the number of time steps per period, $p = T/\Delta t$, assumed to be an integer.

3 Method of stability analysis

The proposed approaches for stability analysis will be presented for periodic systems only because constant coefficient systems are a particular case of periodic systems featuring an arbitrary period.

3.1 Floquet's Theory

Floquet's theory assesses the stability characteristics of general dynamic systems described by eq. (2) with periodic coefficients. Floquet's theory [4,5] involves the *transition matrix*, $\Phi(t)$, that relates the states of the system at time t and $t+T$, $\underline{u}(t+T) = \Phi(t)\underline{u}(t)$. When $t = k\Delta t$, this discrete relationship becomes

$$\underline{u}_{k+p} = \Phi_k \underline{u}_k. \tag{7}$$

The relationship between matrices Φ_k and A_k is found from the discrete time model, eq. (6), as $\Phi_k = A_{k+p-1} A_{k+p-2} \ldots A_k$. An explicit expression for Φ_k is

$$\Phi_k = P_k e^{\Lambda T} P_k^{-1}; \tag{8}$$

The eigenvalues of the transition matrix are $\exp(\lambda_i T)$, $i = 1, 2, \ldots, 2N$, and assumed to be distinct in this discussion. A complete discussion of the general case of repeated eigenvalues is found in ref. [4]. The stability criterion can now be stated as: the periodic system is stable if and only if the norm of all eigenvalues is smaller than unity: $|\exp(\lambda_i T)| < 1,\ \ i = 1, 2, \ldots, 2N$.

In practice, the transition matrix is constructed by a full set of linearly independent solutions $\underline{u}_p^{(i)}$, $i = 1, 2, \ldots, 2N$, when initial conditions are given by the identity matrix,

$$\Phi_0 = \left[\underline{u}_p^{(1)}, \underline{u}_p^{(2)}, \ldots, \underline{u}_p^{(2N)}\right]. \tag{9}$$

This discussion clearly shows the difficulties associated with the application of Floquet's theory for stability assessment. In numerical applications, the evaluation of the transition matrix becomes an overwhelming task as it requires the integration of the system of equations for an entire period, for each degree of freedom of the system. As the number of degrees of freedom of the system increases, this computational effort becomes prohibitive. Furthermore, for larger systems, the transition matrix becomes increasingly ill conditioned.

The last step of Floquet's theory involves the determination of the characteristic exponents of the system from the eigenvalues of the transition matrix. A typical eigenvalue is written as $r_i \exp(\pm \mathbf{i}\phi_i)$, where $\mathbf{i} = \sqrt{-1}$, and a characteristic exponent as $\lambda_i = \omega_i[\zeta_i \pm \mathbf{i}\sqrt{1-\zeta_i^2}]$, where ω_i and ζ_i are the frequency and damping, respectively, associated with this characteristic exponent; it then follows that

$$\zeta_i = \sqrt{\frac{c_i^2}{1+c_i^2}}; \quad \omega_i = \frac{c_i \phi_i}{\zeta_i T}, \quad i = 0, 1, 2, \ldots, N-1, \tag{10}$$

where $c_i = (\ln r_i)/\phi_i$.

3.2 The partial Floquet approach

In view of the high computational cost associated with the application of Floquet's theory, it is desirable to construct an approximation of the transition matrix. In partial Floquet theory [30,31], information about the dynamics of the system is extracted from the response of a small number of degrees of freedom. According to eq. (5), the response of a single degree of freedom of the system can be written as $h(t) = L(t)\exp(\Lambda t)P^{-1}(0)\underline{u}_0$, where array $L(t)$ represents a single line of matrix $P(t)$, and hence, $L(t) = L(t+T)$; $h(t)$ can be viewed as a "sensor" output such as the time history generated by a strain gauge or accelerometer attached to the system. In view of eq. (5), the discretized signal at time $t = k\Delta t + \ell T$, denoted $h_{k,\ell} = h(k\Delta t + \ell T)$, now becomes

$$h_{k,\ell} = L_k e^{\Lambda(k\Delta t + \ell T)} P_0^{-1} \underline{u}_0, \tag{11}$$

where $L_k = L(k\Delta t + \ell T) = L(k\Delta t)$; the last equality follows from the periodic nature of $L(t)$. m consecutive data points starting in the ℓ^{th} period are stored in array $\underline{h}_\ell^T = \lfloor h_{1,\ell} \quad h_{2,\ell} \quad \ldots \quad h_{m,\ell} \rfloor$; if $m < p$, this array stores fewer than the total number of data points in a period, whereas if $m > p$, it stores more than the total number of data points in

a period. Matrix R is now defined

$$R = \begin{bmatrix} L_1 e^{\Lambda \Delta t} \\ L_2 e^{\Lambda 2 \Delta t} \\ \vdots \\ L_m e^{\Lambda m \Delta t} \end{bmatrix}. \tag{12}$$

With the help of this notation, it is clear that $\underline{h}_\ell = R \exp(\Lambda \ell T) P_0^{-1} \underline{u}_0$. The relationship between arrays $\underline{h}_{\ell+1}$ and $\underline{h}_\ell$ is now written in terms of the *transition matrix*, Q, as

$$h_{\ell+1} = Q h_\ell, \quad Q = R e^{\Lambda T} R^+, \tag{13}$$

where R^+ is the Moore-Penrose inverse [32] of R; the superscript $()^+$ will be used here to denote Moore-Penrose inverses.

The following two matrices are now defined

$$H_{0(m\times n)} = [\underline{h}_0 \quad \underline{h}_1 \quad \dots \quad \underline{h}_{n-1}], \quad \text{and} \quad H_{1(m\times n)} = [\underline{h}_1 \quad \underline{h}_2 \quad \dots \quad \underline{h}_n]. \tag{14}$$

Since eq. (13) holds for each column of these matrices, it follows that

$$H_1 = Q H_0. \tag{15}$$

This relationship does not allow the exact computation of the transition matrix, Φ, defined by eq. (7). Indeed, complete knowledge of this matrix requires the responses of all degrees of freedom to $2N$ linearly independent initial conditions, as expressed by eq. (9); if this information were available, matrices H_0 and H_1 of size $2N \times 2N$ could be constructed and $\Phi = H_1 H_0^{-1}$ would yield the transition matrix. In view of the limited information available, an approximation to the transition matrix is evaluated as $Q = H_1 H_0^+$, where the Moore-Penrose inverse [32] of H_0 is evaluated using the singular value decomposition as $H_0^+ = V_r \Sigma_r^{-1} U_r^T$, see Appendix A, where r is the estimated rank of H_0. The estimated transition matrix becomes

$$Q_{(m\times m)} = H_1 V_r \Sigma_r^{-1} U_r^T. \tag{16}$$

In view of its definition in eq. (14), matrix H_0 will store highly redundant data and it is not unexpected that, more often than not, $r < m$. It follows that of the m eigenvalues of Q in eq. (16), r only are expected to be physically meaningful, whereas the remaining $m - r$ eigenvalues are related to noise in the data. Consequently, it makes sense to project matrix Q in the subspace defined by the r proper orthogonal modes of H_0, stored in U_r, to find

$$\hat{Q}_{(r\times r)} = U_r^T Q U_r = U_r^T H_1 V_r^T \Sigma_r^{-1}. \tag{17}$$

The stability characteristics of the system are then extracted from the eigenvalues of the approximate transition matrices, Q or $\hat{Q}$, using eq. (10).

The method presented thus far is based on the information extracted from a single signal, see eq. (11). In practice, if N_s signals are available, the following matrices are constructed

$$\mathbb{H}_0 = \begin{bmatrix} H_0^{(1)} \\ H_0^{(2)} \\ \vdots \\ H_0^{(N_s)} \end{bmatrix}, \quad \mathbb{H}_1 = \begin{bmatrix} H_1^{(1)} \\ H_1^{(2)} \\ \vdots \\ H_1^{(N_s)} \end{bmatrix}; \tag{18}$$

where matrices $H_0^{(k)}$ and $H_1^{(k)}$ are constructed with the data of the k^{th} signal, as defined in eq. (14). The analysis then proceeds as before, with matrices $\mathbb{H}_0$ and $\mathbb{H}_1$ replacing matrices H_0 and H_1, respectively. If the responses of all degrees of freedom of the system are used for stability assessment, Hankel matrices $\mathbb{H}_0$ and $\mathbb{H}_1$ become equivalent to the snapshot matrices and the present partial Floquet theory becomes equivalent to the Poincaré mapping technique [10,12,13].

3.3 The autoregressive approach

The autoregressive method will be presented here as a modification of the partial Floquet approach: by analogy to eq. (15), matrix B is defined as

$$H_1 = H_0 B. \tag{19}$$

Clearly, matrix B and the transition matrix are closely related since $B = H_0^+ Q H_0$. As was the case for the partial Floquet method, too little information is contained in matrices H_0 and H_1 to afford an exact evaluation of B. Hence, the Moore-Penrose inverse of matrix H_0 is used here again to evaluate an approximation as $B = H_0^+ H_1$, and finally,

$$B_{(n\times n)} = V_r \Sigma_r^{-1} U_r^T H_1; \tag{20}$$

In view of highly redundant nature of the data stored in matrix H_0, it should be expected that, in general, $r < n$, and hence, only r eigenvalues of B should be physically meaningful. Consequently, it makes sense to project matrix B in the subspace defined by V_r, to find

$$\hat{B}_{(r\times r)} = V_r^T B V_r = \Sigma_r^{-1} U_r^T H_1 V_r. \tag{21}$$

The stability characteristics of the system are then extracted from the eigenvalues of the approximate transition matrices, B or $\hat{B}$, using eq. (10). Bauchau and Wang [9] have shown that the complex exponential [33] or Prony's method is, in fact, an autoregressive method. Autoregressive methods are often combined with moving average techniques to yield the ARMA algorithm [34]. However, when dealing with stability problems, the excitation of the system often comes in the form of an initial impulse. The moving average component of the ARMA algorithm then automatically vanishes, simplifying to the present autoregressive approach.

The stability analysis algorithms presented in this section produce estimates of r characteristic exponents of the system. The analyst is now faced with the following dilemma: how reliable are these estimates? Poor estimates are due to two broad categories of errors. First, if the excitation of the system is chosen inappropriately, some relevant modes might not be excited, and no matter what signals are used for stability analysis, the dynamics associated with such modes cannot possibly be extracted by any algorithm. Exact evaluation of the characteristic exponents requires the response of all modes to $2N$ linearly independent initial conditions, *i.e.* all modes must be excited to obtain the exact solution. Second, assuming that all relevant modes have sufficient excitation, the noise in the data or a poor choice of signals might lead to inaccurate estimates of system dynamics. Error from the first source cannot be remedied by better algorithms, rather, a better judgement is required of the analyst. Note that this problem is also present when running an experiment: the excitation device must be properly designed to provide enough energy to all relevant modes.

Errors from the second source can be alleviated by better algorithms; two complementary approaches are presented here. The first approach eliminates the need to select specific signals as input to the stability analysis by using all the available data, *i.e.* the responses of all degrees of freedom of the system. While this approach certainly eliminates the guesswork, it will require the singular value decomposition of very large matrices, resulting in large computational costs. The proper orthogonal decomposition method is proposed as a solution of this problem, as discussed in section 4. The second approach relies on the reconstruction or synthesis of the signals associated with the estimates of r characteristic exponents of the system. If the reconstructed signals are in close agreement with the original signals, it is likely that the identified characteristic exponents are reliable estimates. This method is presented in section 5. The combination of these two approaches is expected to yield more reliable estimates of stability characteristics, and warn the analyst when poor predictions are obtained.

4 Use of proper orthogonal modes

When applying the stability algorithms described in section 3 to numerical systems, the responses of all degrees of freedom of the system are available as a result of the computation. This contrasts with experimental applications where only a small number of signals are available. To extract the most accurate predictions, it is logical to use all available data, *i.e.* in eq. (18), the number of signals equals the number of degrees of freedom of the system, $N_s = 2N$. Clearly, in view of its size, the singular value decomposition of matrix $\mathbb{H}_{0(2Nm\times n)}$ will be very expensive.

To bypass this high cost, a preprocessing step, based on the proper orthogonal decomposition, is used to condense the available data. This technique provides a unique decomposition of system response in terms of a set of orthogonal modes associated with decreasing energy content. The few proper orthogonal modes with the highest energy content are then selected to be "generalized" or "optimized sensors" to drive the stability analysis. To implement this

approach, the following matrix is assembled from the time histories of all degrees of freedom

$$T_0 = [\underline{u}_0 \quad \underline{u}_1 \quad \dots \quad \underline{u}_n], \tag{22}$$

where array $\underline{u}_k$ stores all the degrees of freedom of the system at time t_k. Here again, the singular value decomposition is used to compute the proper orthogonal modes of T_0 as $T_0 = U_r \Sigma_r V_r^T$, where U_r stores the proper orthogonal modes, and r is the estimated rank of T_0. The system response is then projected onto the space of the proper orthogonal modes to find the r signals, $U_r^T T_0 = \Sigma_r V_r^T$, or

$$\underline{\mathfrak{h}}_i = \sigma_i \underline{v}_i, \quad i = 1, 2, \dots, r, \tag{23}$$

where $\underline{v}_i$ is the i^{th} column of V_r. The r signals, $\underline{\mathfrak{h}}_i$, are generalized, or optimized signals: while they are not the response of any specific degree of freedom of the system, they form a set of r orthogonal signals containing most of the energy of the system, as measured by the index defined in eq. (A3).

The singular value decomposition of matrix T_0 of size $2N \times n$ is an expensive operation, the cost of which is estimated to be $\mathcal{O}(4N^2 n + n^3)$, see references [35,36]. However, in the present application, it is not necessary to extract all the singular values of T_0, rather, only the r dominant singular values are required. Several algorithms have been proposed for this task [37,38], but one of the most effective tool is the Lanczos algorithm [32] that operates on the following real symmetric matrix

$$\mathbb{T} = \begin{bmatrix} 0 & T_0 \\ T_0^T & 0 \end{bmatrix}. \tag{24}$$

It produces the r dominant singular values and the matrices U_r and V_r at a reasonable computational cost.

5 Signal synthesis

Because of noise in the data or the possibility of a poor choice of signals, the algorithms described above can lead to inaccurate estimates of system dynamics. To detect eventual problems, it is important to reconstruct or synthesize the signals associated with the r estimated characteristic exponents of the system. Let h_k and $\hat{h}_k$ be the original and reconstructed signals, respectively; the discrepancy between the two is quantified by the following index

$$\epsilon = \sqrt{\frac{1}{n} \sum_{k=1}^{n} (\hat{h}_k - h_k)^2}. \tag{25}$$

If the reconstructed signals are in close agreement with the original signals, *i.e.* if ϵ is small, it is likely that the identified characteristic exponents are reliable estimates.

The response of a degree of freedom of the system, $h(t)$, can be expressed in terms of the characteristic exponents as $h(t) = \sum_{j=1}^{2N} \ell_j(t) \exp(\lambda_j t) c_j$, where $\ell_j(t)$ and c_j are the j^{th} elements of arrays $L(t)$ and $\underline{c} = P_0^{-1} \underline{u}_0$, respectively. This expression is further simplified by defining $a_j(t) = \ell_j(t) c_j$, to find $h(t) = \sum_{j=1}^{2N} a_j(t) \exp(\lambda_j t)$. Note that for the actual signal, the summation extents over all $2N$ characteristic exponents of the system; on the other hand, the estimated signal is $\hat{h}(t) = \sum_{j=1}^{r} \hat{a}_j(t) \exp(\hat{\lambda}_j t)$, where the summation extends over the r estimated characteristic exponents, $\hat{\lambda}_j$. Among the r estimated exponents, a null exponent often occurs, corresponding to an offset of the signal, n_r real exponents might appear, and finally, $2n_c$ complex conjugate exponents are also likely to occur. When the characteristic exponents are written as $\exp(\hat{\lambda}_j \Delta t) = r_j \exp(\mathbf{i}\phi_j)$ and the coefficients of the expansion as $\hat{a}_j(t) = \alpha_j(t) + \mathbf{i}\beta_j(t)$, the estimated signal becomes

$$\hat{h}(t) = \alpha_0(t) + \sum_{j=1}^{n_r} \alpha_j(t) r_j^{t/\Delta t} + \sum_{j=n_r+1}^{n_r+n_c} \left[2\alpha_j(t) r_j^{t/\Delta t} \cos(\frac{\phi_j t}{\Delta t}) - 2\beta_j(t) r_j^{t/\Delta t} \sin(\frac{\phi_j t}{\Delta t}) \right]. \quad (26)$$

At time $t = k\Delta t$, the discrete value of the estimated signal is

$$\hat{h}_k = \alpha_{0,k} + \sum_{j=1}^{n_r} \alpha_{j,k} r_j^k + \sum_{j=n_r+1}^{n_r+n_c} \left[2\alpha_{j,k} r_j^k \cos(k\phi_j) - 2\beta_{j,k} r_j^k \sin(k\phi_j) \right] = \underline{q}_k^T \underline{a}_k, \quad (27)$$

where the subscript k indicates a quantity computed at time t_k, and the two arrays $\underline{a}_k$ and $\underline{q}_k$ were defined as

$$\underline{a}_k = \begin{bmatrix} \alpha_{0,k} \\ \alpha_{1,k} \\ \vdots \\ \alpha_{n_r,k} \\ \alpha_{n_r+1,k} \\ \beta_{n_r+1,k} \\ \vdots \\ \alpha_{n_r+n_c,k} \\ \beta_{n_r+n_c,k} \end{bmatrix}, \quad \text{and} \quad \underline{q}_k = \begin{bmatrix} 1 \\ r_1^k \\ \vdots \\ r_{n_r}^k \\ 2r_{n_r+1}^k \cos(k\phi_{n_r+1}) \\ -2r_{n_r+1}^k \sin(k\phi_{n_r+1}) \\ \vdots \\ 2r_{n_r+n_c}^k \cos(k\phi_{n_r+n_c}) \\ -2r_{n_r+n_c}^k \sin(k\phi_{n_r+n_c}) \end{bmatrix}, \quad (28)$$

respectively, and $\alpha_{j,k} = \alpha_j(k\Delta t)$. Array $\underline{q}_k$ stores known quantities related to the estimated exponents and $\underline{a}_k$ the unknown coefficients of the expansion of the estimated signal. Floquet's theory implies that $a_j(t)$ is a periodic function and hence, $\underline{a}_k = \underline{a}_{k+p}$. The unknown coefficients of the expansion are now computed by matching the actual and estimated signals

at discrete time steps $t_{k+\ell p}$, $h_{k+\ell p} = \hat{h}_{k+\ell p}$, $\ell = 0, 1, \ldots, m$, to find

$$\begin{bmatrix} h_k \\ h_{k+p} \\ \vdots \\ h_{k+mp} \end{bmatrix} = \begin{bmatrix} \underline{q}_k^T \\ \underline{q}_{k+p}^T \\ \vdots \\ \underline{q}_{k+mp}^T \end{bmatrix} \underline{a}_k = \mathcal{Q}_k \ \underline{a}_k. \tag{29}$$

This set of linear equations is solved using the least square method, such that

$$\underline{a}_k = (\mathcal{Q}_k^T \mathcal{Q}_k)^{-1} \mathcal{Q}_k \begin{bmatrix} h_k \\ h_{k+p} \\ \vdots \\ h_{k+mp} \end{bmatrix}. \tag{30}$$

Solving this linear system for $k = 0, 1, 2, \ldots p-1$, will yield discrete values of the periodic coefficients of the expansion, $a_j(t)$, over one period. Of course, for constant coefficient systems, the procedure simplifies considerably, since the coefficients of the expansion become constants. Once the coefficients of the expansion are evaluated, the estimated signal, $\hat{h}$, follows from eq. (27) and the quality of the estimation can be assessed with the help of eq. (25). The evaluation of the estimated signal is particularly important for periodic systems: if the sole information available is the characteristic exponent, an indeterminacy remains concerning the corresponding system frequency. Indeed, the contribution of the exponent to system response is of the form $a_j(t)\exp(\lambda_j)$, where $a_j(t)$ is a periodic function. Expanding a_j in Fourier series yields $a_j(t) = \sum_k g_{jk} \exp(\mathbf{i}k\Omega t)$, where $\Omega = 2\pi/T$, and hence, the frequency of the system becomes $\omega_j\sqrt{1-\zeta_j^2} + k\Omega$, where k is an undetermined integer. If the estimated signal is evaluated, $a_j(t)$ is known in discrete form and so are its Fourier coefficients, g_{jk}. The non vanishing coefficients g_{jk} determine the integers k.

6 Stability analysis procedure

The algorithms described in the last two sections are combined to provide a robust approach to the stability analysis of complex systems. The overall procedure involves the following steps.

(1) Determine the dynamic response of the system to a given excitation.
(2) Construct matrices T_0 and $\mathbb{T}$ defined in eq. (22) and eq. (24), respectively.
(3) Evaluate $r_{\mathbb{T}}$ proper orthogonal modes from matrix $\mathbb{T}$ using Lanczos algorithm.
(4) Compute the $r_{\mathbb{T}}$ optimal signals defined by eq. (23).
(5) From these signals, assemble matrices $\mathbb{H}_0$ and $\mathbb{H}_1$ defined by eq.(14).
(6) Perform the singular value decomposition of $\mathbb{H}_0$.

(7) Evaluate matrix $\hat{Q}$ or $\hat{B}$ using eq. (17) or (21), and compute its eigenvalues.
(8) Compute the associated system frequencies and damping using eq. (10).
(9) Compute the coefficients of the expansion, $\underline{a}_k$, using eq.(30)
(10) Evaluate the estimated signal, $\hat{h}_k$, using eq.(27).

The above procedure calls for the following remarks.

(1) The procedure presented above is equally applicable for constant coefficient and periodic systems. In the former case, many of the steps of the procedure considerably simplify.
(2) The first step of the procedure is critical as it involves the selection of a suitable excitation. The excitation should provide an adequate amount of energy for the modes of interest, typically, the least damped modes of the system. Clearly, this step requires the understanding of the dynamic behavior of the system.
(3) Steps 2, 3 and 4 can be bypassed and replaced by a choice of suitable signals, typically the response of specific degrees of freedom of the system. The computation of the proper orthogonal decomposition and associated optimal signals relieves the analyst from having to select suitable signals, leading to a more robust procedure.
(4) Step 3 and 7 involves the estimations of the rank of matrices $\mathbb{T}$ and $\mathbb{H}_0$, respectively; these are crucial steps of the procedure. The energy index, eq. (A3), is conveniently used for this estimation by requiring $E_{r_{\mathbb{T}}} > 1 - \epsilon$ and $E_{r_{\mathbb{H}_0}} > 1 - \epsilon$, where ϵ is a small, user defined number. It is sometimes convenient to let $r_{\mathbb{T}}$ and $r_{\mathbb{H}_0}$ be user specified inputs.

7 Numerical examples

Three examples will be treated in this section, illustrating the various methods described in this paper.

7.1 Parametric excitation of a beam

The first example deals with a uniform, simply supported beam of length $\ell = 1$ m subjected to an end compressive load of harmonically varying amplitude, $P = P_0 + P_1 \cos(\omega_p t)$. The physical properties of the beam are: bending stiffness, $EI = 6.57$ kN·m^2 and mass per unit span, $m = 3.24$ kg/m.

The governing equation of the problem is readily derived with the help of the Euler-Bernoulli assumptions to find

$$EI\frac{\partial^4 w}{\partial x^4} + (P_0 + P_1 \cos\omega_p t)\frac{\partial^2 w}{\partial x^2} + c\frac{\partial w}{\partial t} + m\frac{\partial^2 w}{\partial t^2} = 0, \tag{31}$$

where w is the transverse displacement of the beam and c the damping coefficient. Analytical solutions of the problem are obtained with the variable separation method [1]. The

transverse displacement of the beam is expanded as $w(x,t) = q_k(t) \sin k\pi x/\ell$, $k = 1, 2, \ldots, n$. Substituting this assumed solution into the governing equation then yields

$$\ddot{q}_k + \epsilon \dot{q}_k + \Omega_k^2 (1 - \frac{P_0 + P_1 \cos \omega_p t}{P_k}) q_k = 0 \tag{32}$$

where $\Omega_k = (k\pi/\ell)^2 \sqrt{EI/m}$ is the $k^{\texttt{th}}$ natural frequency of the beam, $P_k = (k\pi/\ell)^2 EI$ Euler's $k^{\texttt{th}}$ buckling load, and $\epsilon = c/m$. For convenience, eq. (32) is rewritten as $\ddot{q}_k + \epsilon \dot{q}_k + \omega_k^2 (1 - 2\mu_k \cos \omega_p t) q_k = 0$, where $\omega_k = \Omega_k \sqrt{1 - P_0/P_k}$ and $\mu_k = 1/2 \; P_1/(P_k - P_0)$. Finally, this equation is brought in the form of the well-known Mathieu equation [5] by non dimensionalizing all terms to find $\mathrm{d}^2 q_k/\mathrm{d}\tau^2 + \hat{\epsilon} \mathrm{d} q_k/\mathrm{d}\tau + (a - 2q \cos 2\tau) q_k = 0$, where $\tau = \omega_p t/2$, $\hat{\epsilon} = 2\epsilon/\omega_p$, $a = (2\omega_k/\omega_p)^2$ and $q = a\mu/2$. The harmonic balance method provides a classical solution of this equation and the stability boundaries for the problem are computed via Hill's infinite determinant approach. Fig. 1 shows Strutt's diagram that depicts the stability boundaries in the space of the excitation frequency, $\omega = \omega_p/(2\omega_k)$, versus excitation parameter, $\mu = \mu_k$, in the absence of damping.

The stability analysis method proposed in this paper will be validated by comparing predicted stability boundaries with those obtained via Hill's infinite determinant method and predicted frequencies and damping with those extracted from a direct application of Floquet's classical theory. The beam was modeled with 4 cubic finite elements [39]; the numerical simulation was run for a total of 12 periods, $T = 2\pi/\omega_p$, with a time step $\Delta t = 1.0$ msec. For the stability analysis, the sampling period was set to $T/96$, 3 proper orthogonal modes containing over 95% of the system's energy were used as optimized signals, and the characteristics of the system were estimated using matrix $\hat{Q}$, see eq. (17). Fig. 1 shows that excellent correlation is found between the predictions of Hill's determinant and of the proposed approach. For a more quantitative comparison of the predictions, Fig. 2 shows the frequency and damping associated with the characteristic exponent of largest magnitude as a function of excitation frequency, for an excitation parameter $\mu = 0.15$. Finally, the last part of the figure compares the norms of the maximum eigenvalue of the transition matrix. Excellent agreement is found for all results.

Next, the effect of damping on stability boundaries was investigated. Damping was modeled by adding to the simulation viscous forces proportional to the strain rates, $\underline{F}_d = \mu_s K_s \dot{\underline{e}}$, where μ_s is the damping coefficient, $\underline{e}$ the strain array, and K_s the beam cross-sectional stiffness matrix. These quantities are all measured in a cross-section attached coordinate system. Fig. 3 shows the stability boundaries in the presence of damping, as predicted by Hill's infinite determinant and by the present method. The damping coefficient was selected as $\mu_s = 0.2$ msec, which corresponds to $\epsilon = 12.57$ sec^{-1}. Fig. 4 shows the frequency, damping and norm associated with the characteristic exponent of largest magnitude, for an excitation parameter $\mu = 0.15$. Excellent agreement is found for all results.

7.2 Jeffcott rotor with compliant bearings

The Jeffcott rotor is composed of a flexible anisotropic shaft of length $L = 1$ m and of a mid-span rigid disk of mass $M = 5$ kg and radius $R = 0.18$ m, as shown in Fig. 5. The shaft, modeled by six equally spaced cubic beam elements, is connected to end flexible couplings, represented by concentrated spring. The finite stiffness end bearings consist of revolute joints connected to the ground by concentrated springs. The relative rotation of the left hand side revolute joint was prescribed to be a constant angular velocity Ω.

The sectional properties of the shaft are as follows: bending stiffness, $EI_2 = 175$ and $EI_3 = 98.9$ N·m^2, mass per unit length $m_s = 0.00475$ kg/m, torsional stiffness $GJ = 71.9$ N·m^2, and polar moment inertial $I_\rho = 1.01\ 10^{-5}$ kg·m^2. The elastic couplings had very low axial stiffness $k_1^c = 10.0$ N/m and bending stiffnesses $c_2^c = c_3^c = 10.0$ N·m/rad but high transverse stiffnesses $k_2^c = k_3^c = 100$ MN/m and torsional stiffness $c_1^c = 100$ MN·m/rad; the elastic bearings have low transverse stiffnesses $k_2^b = k_3^b = 30$ kN/m, high axial stiffness $k_1^b = 100$ MN/m, and high bending stiffnesses $c_1^b = c_2^b = c_3^b = 100$ MN·m/rad. Simulations were run for a total of 10 periods, $T = 2\pi/\Omega$, with a time step $\Delta t = 0.1$ msec, after application of an external perturbation along the $\bar{\imath}_3$ axis, $f_3 = 10\sin(20\pi t)$ for $t \in [0, 50]$ msec, to rigid disk. For the stability analysis, the sampling period is $T/128$ sec and 3 proper orthogonal modes were used. System characteristics were extract from matrix $\hat{Q}$, see eq. (17).

A analytical solution of this problem was obtained based on classical modal reduction techniques. The bending flexibility of the shaft was taken into account, but its torsional flexibility was ignored. Furthermore, since the mid-span rigid disk is much more massive than the shaft, the inertial effects of the shaft were ignored. When the equations of motion for this simplified system are written in a rotating frame of reference, a set of constant coefficient equations results, and classical methods can be used to evaluate stability of the system.

Fig. 6 compares the predictions of the simplified analytical model with those of the proposed approach. Due to the bending stiffnesses anisotropy of the shaft, the system is unstable for angular speeds between the two lowest bending frequencies of the shaft, *i.e.* for $29.2 < \Omega < 37.3$ rad/sec. Note the excellent agreement between the predictions of the two approaches. Fig. 7 shows the original and reconstructed signals for the three generalized signals corresponding the three proper orthogonal modes selected for the stability analysis, at an angular speed $\Omega = 24$ rad/sec. The original and reconstructed are in a good agreement, $\epsilon = 3.99\ 10^{-4}$, $9.10\ 10^{-4}$ and $1.95\ 10^{-4}$ for the three signals, respectively, see eq. (25). Table 1 shows the coefficient of the Fourier transform of a_j associated with the frequency $\omega_j\sqrt{1-\zeta_j^2} = 8.643$ rad/sec extracted from two signals corresponding to the two transverse displacements of the rigid disk. The only non vanishing component of the Fourier transforms corresponds to $k = 1$; this means that the frequency of the system is $\omega_j\sqrt{1-\zeta_j^2} + \Omega$, removing the frequency indeterminacy.

Next, the effect of damping was investigated. Damping in the rotating system was modeled by viscous forces proportional to the strain rates, $\underline{F}_d = \mu_s K_s \underline{\dot{e}}$, where μ_s is the damping

coefficient, $\underline{e}$ the strain array, and K_s the beam cross-sectional stiffness matrix. On the other hand, damping in the non-rotating system was modeled by transverse viscous dampers of constant μ_b in the bearing supports. Fig. 8 compares the predictions of the simplified analytical model and of the present approach, for damping parameters $\mu_s = 1$ msec and $\mu_{b1} = \mu_{b2} = 3$ N·sec/m. For shaft speeds below the stability boundary, the two bending modes are now damped. The fixed and rotating system damping mechanisms have a modest effect on the size of the unstable zone, $29.4 < \Omega < 37.0$ rad/sec, and do not stabilize the system at higher shaft speeds.

In a second set of simulations, the compliant bearing at the right hand side of the shaft was replaced by a spatial clearance element, see Fig. 5(b), which models the clearance between the inner and outer races of a journal bearing, as described by Bauchau and Rodriguez [40]. Intermittent contact is allowed between a disk of radius 80 mm, representing the journal, and a cylinder, of radius 80.8 mm, representing the outer race of the bearing. When the two components are in contact, an elastic contact model is activated that consists of an elastic force, $F^e = 15\ a$ MN/m, where a is the approach between the inner and outer races, and of a dissipative force, $F^d = F^e \mu \dot{a}$, where the damping coefficient $\mu = 1.0\ 10^{-3}$ sec/m.

Due to the intermittent nature of the contact between the inner and outer races, the problem presents severe nonlinearities, and a chaotic response. Clearly, an analytical solution of the problem would be difficult to obtain, and furthermore, any stability analysis approach based on linearization of the equation of motions would be unable to capture the effect of intermittent contact. Indeed, the linearization procedure could be performed about the contacting or non contacting state, but not for intermittent contact. When contact occurs, the modes of the system are those of a simply supported beam, but in the non contacting state, the modes are those of a simply supported-free beam. Fig. 9 shows the frequency and damping of the lowest damped modes of the system. Since no analytical solution is available, the solution of the problem featuring two compliant bearings is presented in dotted lines, for reference. Clearly, the nonlinear behavior of the system greatly affects the stability characteristics of the system. Due to the additional modes of the system stemming from the varying boundary conditions at the spatial clearance joint, additional frequencies and associated dampings are identified for rotor speeds larger than 33 rad/sec. A larger scatter in the predictions is observed, due to the chaotic nature of the response. Note that strictly speaking, the proposed methodology does not apply to nonlinear systems since it is based on Floquet's theory. However, partial Floquet or autoregressive methods are routinely used to reduce experimental data, although they strictly apply to linear systems only. Clearly, the proposed approach closely follows the procedures used to reduce experimental data.

7.3 Flutter of a Rectangular Planform Wing

The last example is an aeroelastic problem dealing with the symmetric flutter of a rectangular planform wing clamped at its mid-point [41]. Due to symmetry, a half configuration was modeled and proper symmetry conditions were applied. This problem involves both struc-

tural and aerodynamic states. The half wing has a rectangular planform of length $L = 20$ ft and chord length $c = 6$ ft. The flutter speed of the wing was experimentally measured as $U_F = 590$ ft/sec. The structural properties of the cantilevered wing are as follows: bending stiffness, $EI = 2.4\ 10^7$ lbs·ft^2, torsional stiffness, $GJ = 2.4\ 10^6$ lbs·ft^2, mass per unit span, $m = 0.75$ slugs/ft, polar moment of inertia, $I_\rho = 1.95$ slugs·ft. The airfoil quarter-chord and center of mass are located 0.5 and 0.6 ft aft the elastic axis of the wing, respectively. The wing semi-span is modeled with four cubic beam elements.

The aerodynamic model combines thin airfoil theory with a three dimensional dynamic inflow model. The airfoil has a constant slope of the lift curve $a_0 = 6.28$, and the moment coefficients about the quarter-chord are zero. The inflow velocities at each span-wise location are computed using the finite state induced flow model developed by Peters *et al.* [42,43]. The number of inflow harmonics was selected as $m = 9$, corresponding to 55 aerodynamic inflow states for this symmetric problem. Airloads were computed at 9 stations along the wing span, located at the positions corresponding to Gaussian quadrature. Selecting larger numbers of aerodynamic states or airloads computation points did not significantly affect the results.

The simulation was run for a total period of 1 sec, using a constant time step $\Delta t = 1$ msec. This example will be used to illustrate the two strategies proposed in this paper: the use of user selected signals and the use of optimized signals based on proper orthogonal modes. In the first case, denoted *case 1*, two signals were used: the three-quarter span transverse displacement and twist of the wing. In the second case, denoted *case 2*, the proper orthogonal modes of the system were first extracted from the response of all the degrees of freedom, the six displacement components at each of the 12 nodes of the structural model, and the airload components at the 9 stations. The criterion $E_{r_\mathbb{T}} > 0.92$ lead to the use of 3 proper orthogonal modes; on the other hand, $r_{\mathbb{H}_0}$ was set to 6, corresponding to $E_{r_{\mathbb{H}_0}} > 0.97$. The signals used for stability analysis spanned the response of the system for $t \in [0.30, 0.95]$ sec, with a sampling period of 2 msec. Fig. 10 shows the frequency and damping of the two modes with the lowest frequencies versus far field flow velocity. This figure is similar to that obtained from the classical, two degree of freedom analysis of a wing section [44]. The lowest bending and torsional modes nearly coalesce at flutter. Note that the higher bending and torsional modes do not appear on the figure, although they are included in the model. This is due to the fact that these modes are heavily damped by the aerodynamic forces, and hence are identified as "noise" by the proposed methods. From fig. 10, the flutter speed is found to be $U_F = 585$ ft/sec, for *cases 1* and *2*; this compares favorably with the experimentally measured flutter speed of 590 ft/sec. For *case 2*, the optimized sensors obtained from the proper orthogonal modes allow a more robust determination of the frequency and damping rates: for air speeds above 520 ft/sec, the predictions based on two signals only are no longer satisfactory for the second mode of the system. It should be noted, however, that both cases predict the same flutter speed. Predictions become less accurate in the unstable regime, due to the nonlinear behavior associated with large deflections of the wing. Furthermore, it becomes increasingly difficult to trace the second mode because it is heavily damped.

For this example, the four stability algorithms presented in this paper, see eqs. (16), (17),

(20) and (21), were used to predict the frequencies and damping of the system for a far field flow velocity $U = 590$ ft/sec. Identical predictions, within four significant digits, were obtained from the eigenvalues of the four matrices.

8 Conclusions

Linearized stability analysis methodologies that are applicable to large scale, multi-physics problems were presented in this paper. The first contribution of this work is the development of two classes of closely related algorithms based on a partial Floquet and on an autoregressive approach, respectively. Second, a number of other approaches, such as Prony's method or Poincaré mapping, have been shown to be identical to those proposed here. The common foundation of all these approaches was emphasized. Third, the robustness of the approach was improved by using optimized signals that are derived from the proper orthogonal modes of the system, a set of orthogonal modes capturing the dominant motion of the system in an energy norm. Even for large systems, proper orthogonal modes can be effectively extracted from the very large set of data represented by the response of all degrees of freedom of the system using the Lanczos algorithm. Finally, signal synthesis based on the identified frequencies and damping rates was shown to be an important tool for assessing the accuracy of the identified parameters; furthermore, it provides a means of resolving the frequency indeterminacy associated with the eigenvalues of the transition matrix for periodic systems. The proposed approaches are computationally inexpensive and consist of purely post processing steps that can be used with any multi-physics computational tool or with experimental data. Unlike classical stability analysis methodologies, the linearization of the equations of motion of the system is not required. In the proposed implementation, the singular value decomposition is systematically used as a means of dealing with noisy, highly redundant data sets.

References

[1] V.V. Bolotin. *Nonconservative Problems of the Theory of Elastic Stability.* Pergamon Press Limited, Oxford, England, 1963.

[2] M.J. Goodwin. *Dynamics of Rotor-Bearing Systems.* Unwinm Hyman, London, 1989.

[3] M. Lalane and G. Ferraris. *Rotordynamics Prediction in Engineering.* John Wiley & Sons, New York, 1990.

[4] H. Hochstadt. *Differential Equations.* Dover Publications, Inc., New York, 1964.

[5] A.H. Nayfeh and D.T. Mook. *Nonlinear Oscillations.* John Wiley & Sons, New York, 1979.

[6] A. Cardona. *An Integrated Approach to Mechanism Analysis.* PhD thesis, Université de Liège, 1989.

[7] A. Cardona and M. Géradin. Time integration of the equations of motion in mechanism analysis. *Computers & Structures*, 33(3):801–820, 1989.

[8] O.A. Bauchau, C.L. Bottasso, and Y.G. Nikishkov. Modeling rotorcraft dynamics with finite element multibody procedures. *Mathematical and Computer Modeling*, 33(10-11):1113–1137, 2001.

[9] O.A. Bauchau and J.L. Wang. Stability analysis of complex multibody systems. *ASME Journal of Computational and Nonlinear Dynamics*, 1(1):71–80, January 2006.

[10] K.D. Murphy, P.V. Bayly, L.N. Virgin, and J.A. Gottwald. Measuring the stability of periodic attractors using perturbation induced transients: Applications to two nonlinear oscillators. *Journal of Sound and Vibration*, 172:85–102, 1994.

[11] S.T. Trickey, L.N. Virgin, and E.H. Dowell. The stability of limit cycle oscillations in a nonlinear aeroelastic system. *Proceedings of the Royal Society of London*, 458:2203–2226, 2002.

[12] G. Quaranta, P. Mantegazza, and P. Masarati. Assessing the local stability of periodic motions for large multibody non-linear systems using proper orthogonal decomposition. *Journal of Sound and Vibration*, 271:1015–1038, 2004.

[13] D.P. Lathrop and E.J. Kostelich. Characterization of an experimental strange attractor by periodic orbits. *Physical Review A*, 40(7):4028–4031, 1989.

[14] A.C. Antoulas, D.C. Sorensen, and S. Gugercin. A survey of model reduction methods for large scale systems. *Contemporary Mathematics, AMS Publication*, 280:193–219, 2001.

[15] B. Ho and R. Kalman. Efficient construction of linear state variable models from input/output functions. *Regelungstechnik*, 14:545–548, 1966.

[16] J.N. Juang and R.S. Pappa. An eigensystem realization algorithm for modal parameter identification and model reduction. *Journal of Guidance, Control, and Dynamics*, 8(5):620–627, 1985.

[17] B.C. Moore. Principal component analysis in linear systems: Controllability, observability, and model reduction. *IEEE Transaction on Automatic Control*, AC-26(1):17–32, 1981.

[18] S. Gugercin and A.C. Antoulas. A survey of model reduction by balanced truncation and some new results. *International Journal of Control*, 77(8):748–766, 2004.

[19] J. Durbin. Efficient estimation of parameter in moving average models. *Biometrica*, 46:306–316, 1959.

[20] S.M. Kay and V. Nagesha. Maximum likelihood estimation of signals in autoregressive noise. *IEEE Transactions on Signal Processing*, 42(1):88–101, 1994.

[21] P.E. Gautier, C. Gontier, and M. Smail. Robustness of an arma identification method for modal analysis of mechanical systems in the presence of noise. *Journal of Sound and Vibration*, 179(2):227–242, 1995.

[22] K. Glover. All optimal Hankel-norm approximations of linear multivariable systems and their L inf-error bounds. *International Journal of Control*, 39(4):1115–1193, 1984.

[23] K. Shin, J.K. Hammon, and P.R. White. Iterative svd method for noise reduction of low-dimensional chaotic time series. *Mechanical Systems and Signal Processing*, 13(1):115–124, 1999.

[24] K. Pearson. On lines and planes of closest fit to points in space. *Philosophical Magazine*, 2:609–629, 1901.

[25] T. Lieu, C. Farhat, and M. Lesoinne. Reduced-order fluid/structure modeling of a complete aircraft configuration. *Computer methods in applied mechanics and engineering*, to appear, 2006.

[26] R.A. Bialecki, A.J. Kassab, and A. Fic. Proper orthogonal decomposition and modal analysis for acceleration of transient fem thermal analysis. *International Journal for Numerical Methods in Engineering*, 62(6):774–797, 2005.

[27] S. Lall, J.E. Marsden, and S. Glavaški. A subspace approach to balanced truncation for model reduction of nonlinear control systems. *International Journal of Robust and Nonlinear Control*, 12(5):519–535, 2002.

[28] B.F. Feeny and R. Kappagantu. On the physical interpretation of proper orthogonal modes in vibrations. *Journal of Sound and Vibration*, 211(4):607–611, 1998.

[29] M.F.A. Azeez and A.F. Vakakis. Proper orthogonal decomposition (POD) of a class of vibroimpact oscillations. *Journal of Sound and Vibration*, 240(5):859–889, 2001.

[30] Xin Wang and D.A. Peters. Floquet analysis in the absence of complete information on states and perturbations. In *Proceedings of the Seventh International Workshop on Dynamics and Aeroelasticity Stability Modeling, St. Louis, October 14-16*, pages 237–248, 1997.

[31] D.A. Peters and Xin Wang. Generalized floquet theory for analysis of numerical or experimental rotor response data. In *Proceedings of the 24th European Rotorcraft Forum*, Marseilles, France, September 1998.

[32] G.H. Golub and C.F. Van Loan. *Matrix Computations*. The Johns Hopkins University Press, Baltimore, second edition, 1989.

[33] D.J. Ewins. *Modal testing: theory and practice*. Wiley, New York, 1984.

[34] J. Lardies. Analysis of multivariate autoregressive process. *Mechanical Systems and Signal Processing*, 10(6):747–761, 1996.

[35] J.W. Demmel. *Applied Numerical Linear Algebra*. SIAM, Philadelphia, 1997.

[36] L.N. Trefethen and D. Bau. *III. Numerical Linear Algebra*. SIAM, Philadelphia, 1997.

[37] R.D. Fierro and E.P. Jiang. Lanczos and the riemannian SVD in information retrieval applications. *Numerical Linear Algebra With Applications*, 12:355–372, 2005.

[38] E. Kokiopoulou, C. Bekas, and E. Gallopoulos. Computing smallest singular triplets with implicitly restarted lanczos bidiagonalization. *Applied Numerical Mathematics*, 49:39–61, 2004.

[39] O.A. Bauchau. Computational schemes for flexible, nonlinear multi-body systems. *Multibody System Dynamics*, 2(2):169–225, 1998.

[40] O.A. Bauchau and J. Rodriguez. Modeling of joints with clearance in flexible multibody systems. *International Journal of Solids and Structures*, 39:41–63, 2002.

[41] M. Goland. The flutter of a uniform cantilever wing. *Applied Mechanics*, 12(4):A197–A208, 1945.

[42] D.A. Peters, S. Karunamoorthy, and W.M. Cao. Finite state induced flow models. Part I: Two-dimensional thin airfoil. *Journal of Aircraft*, 32:313–322, 1995.

[43] D.A. Peters and C.J. He. Finite state induced flow models. Part II: Three-dimensional rotor disk. *Journal of Aircraft*, 32:323–333, 1995.

[44] R.L. Bisplinghoff, H. Ashley, and R.L. Halfman. *Aeroelasticity*. Addison-Wesley Publishing Company, Reading, Massachusetts, second edition, 1955.

	g_{j0}	g_{j1}	g_{j2}	g_{j3}
signal 1	0.0045	0.4949	0.0060	0.0091
signal 2	0.0044	0.4146	0.0081	0.0074

Table 1
Magnitude of the Fourier coefficients of a_j for signals 1 and 2.

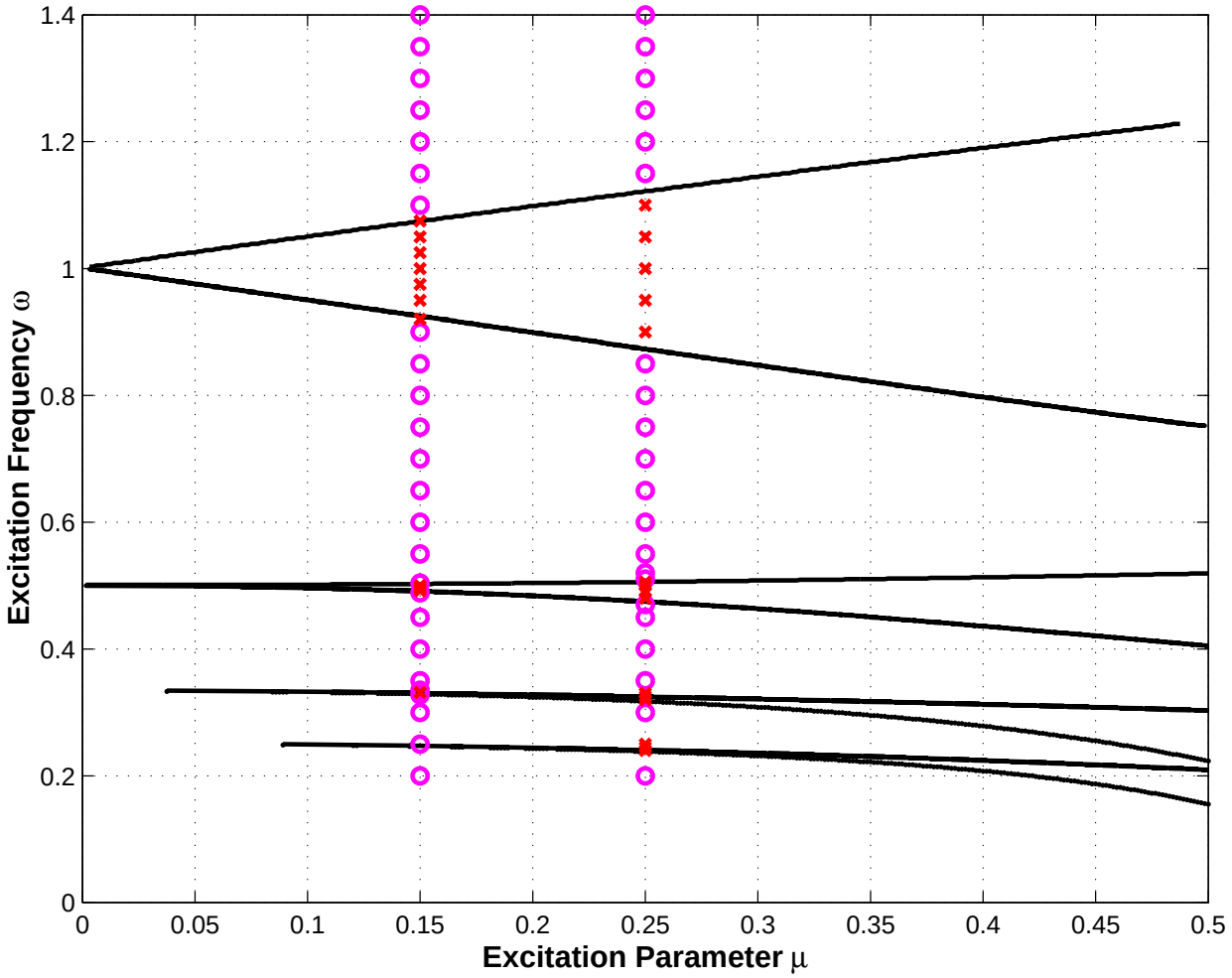

Figure 1. Strutt's diagram. Stability boundaries predicted by Hill's infinite determinant, solid lines. Present predictions for $\mu = 0.15$ and 0.25: stable solution, ($\circ$), unstable solution, ($\times$).

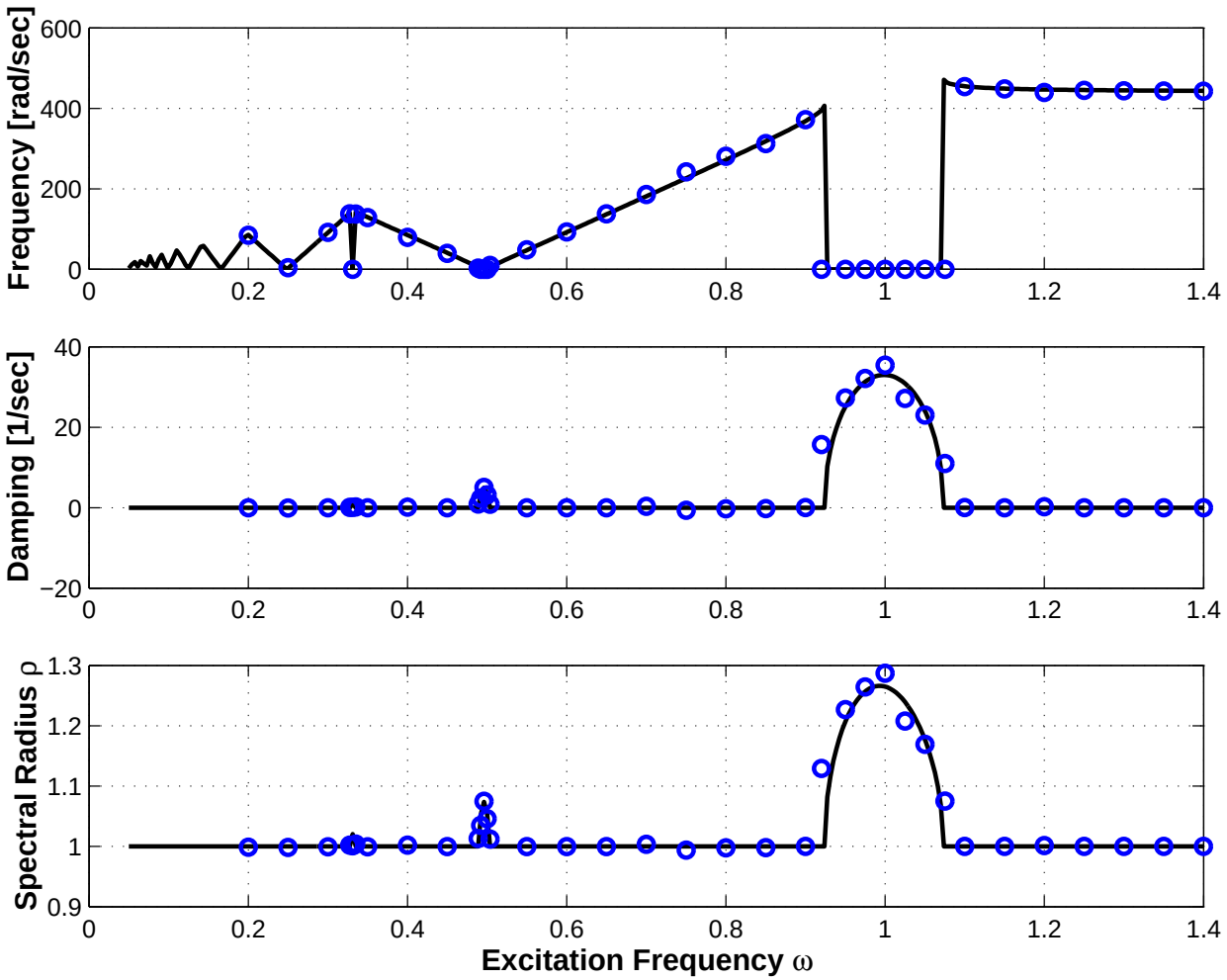

Figure 2. Frequency (top figure), damping (middle figure) and norm (bottom figure) of the maximum eigenvalue of the system versus excitation frequency, for $\mu = 0.15$. Floquet's classical analysis: solid line; present approach: ($\circ$).

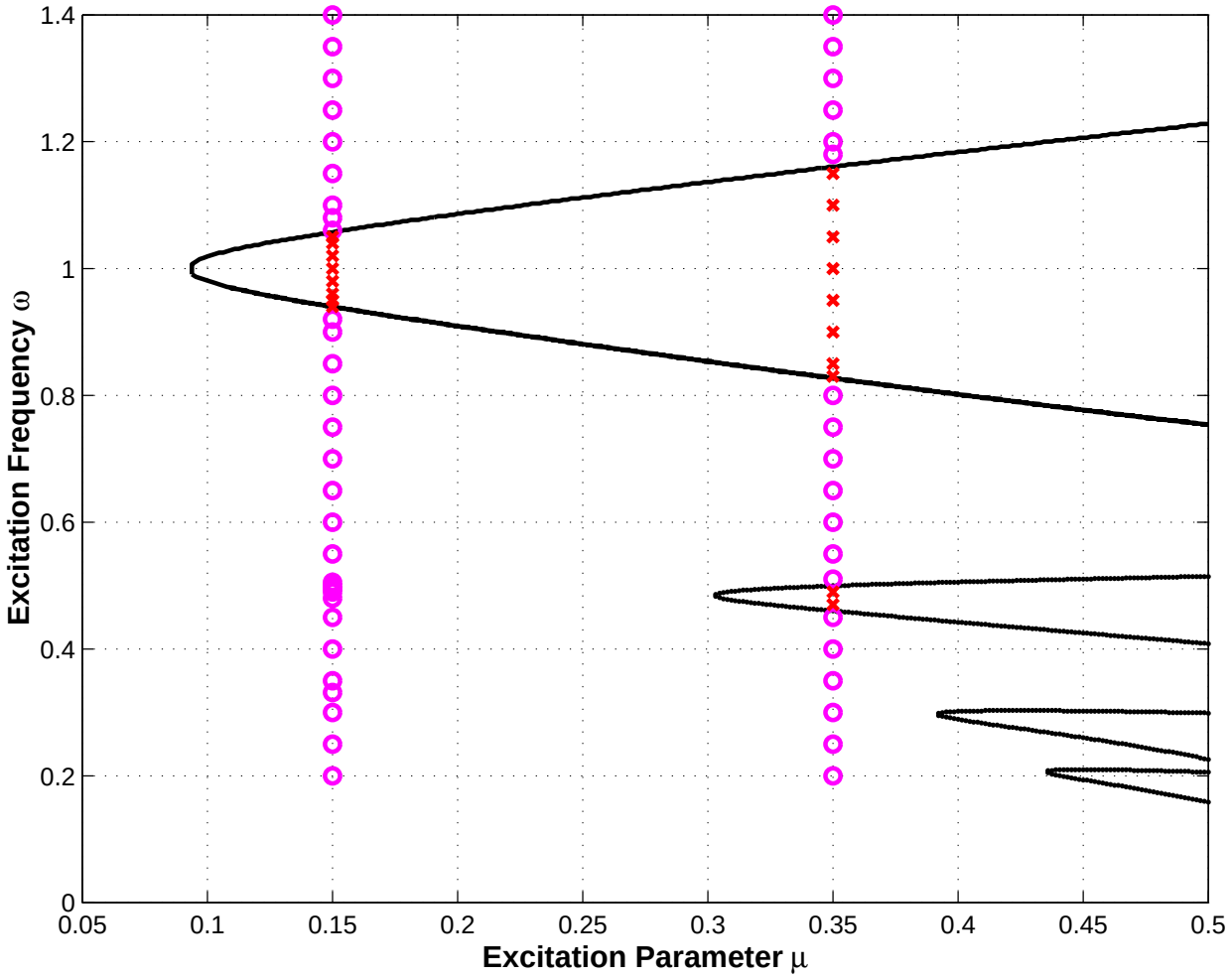

Figure 3. Strutt's diagram. Stability boundaries predicted by Hill's infinite determinant, solid lines. Present predictions for $\mu = 0.15$ and 0.25: stable solution, ($\circ$), unstable solution, ($\times$).

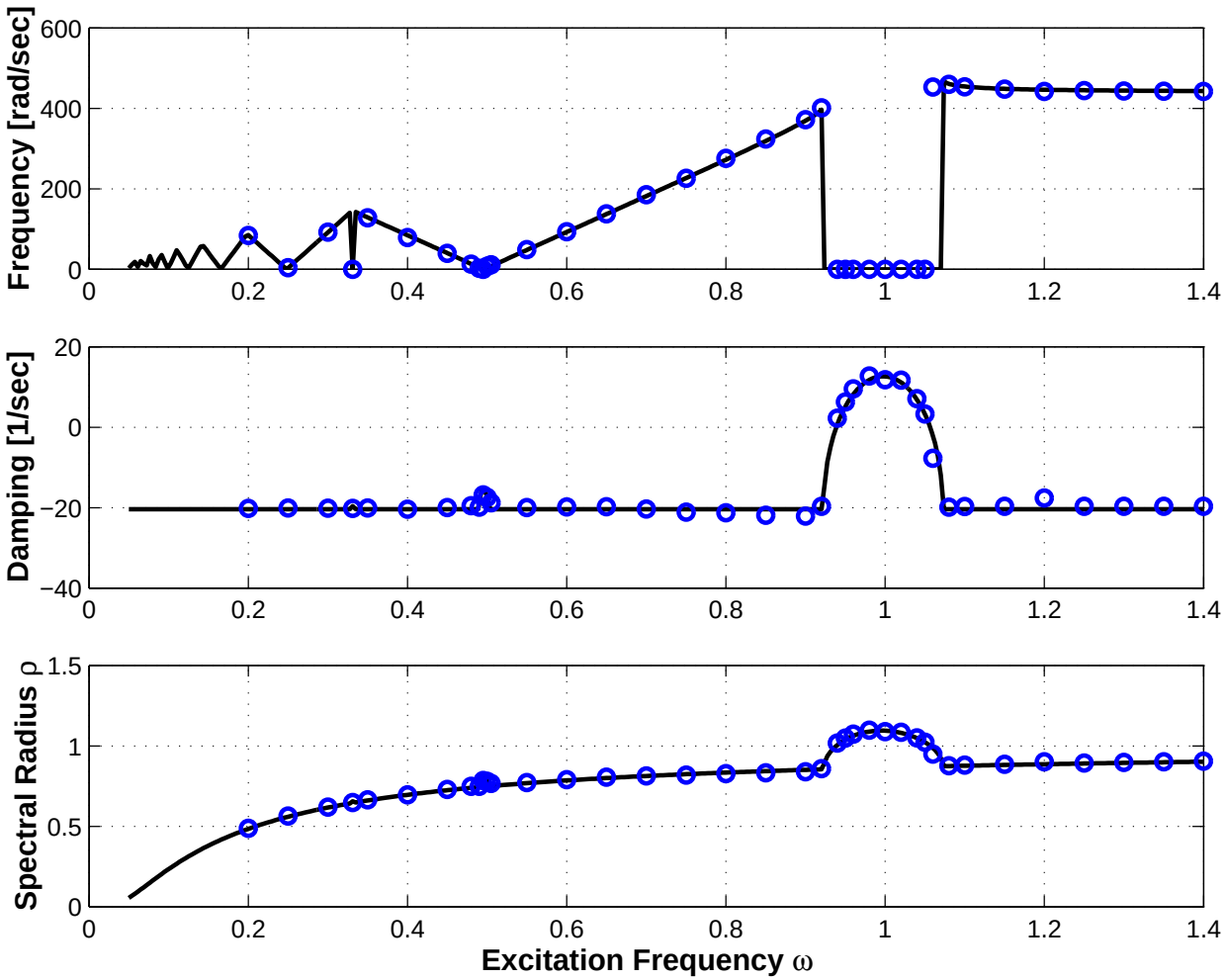

Figure 4. Frequency (top figure), damping (middle figure) and norm (bottom figure) of the maximum eigenvalue of the system versus excitation frequency, for $\mu = 0.15$. Floquet's classical analysis: solid line; present approach: ($\circ$).

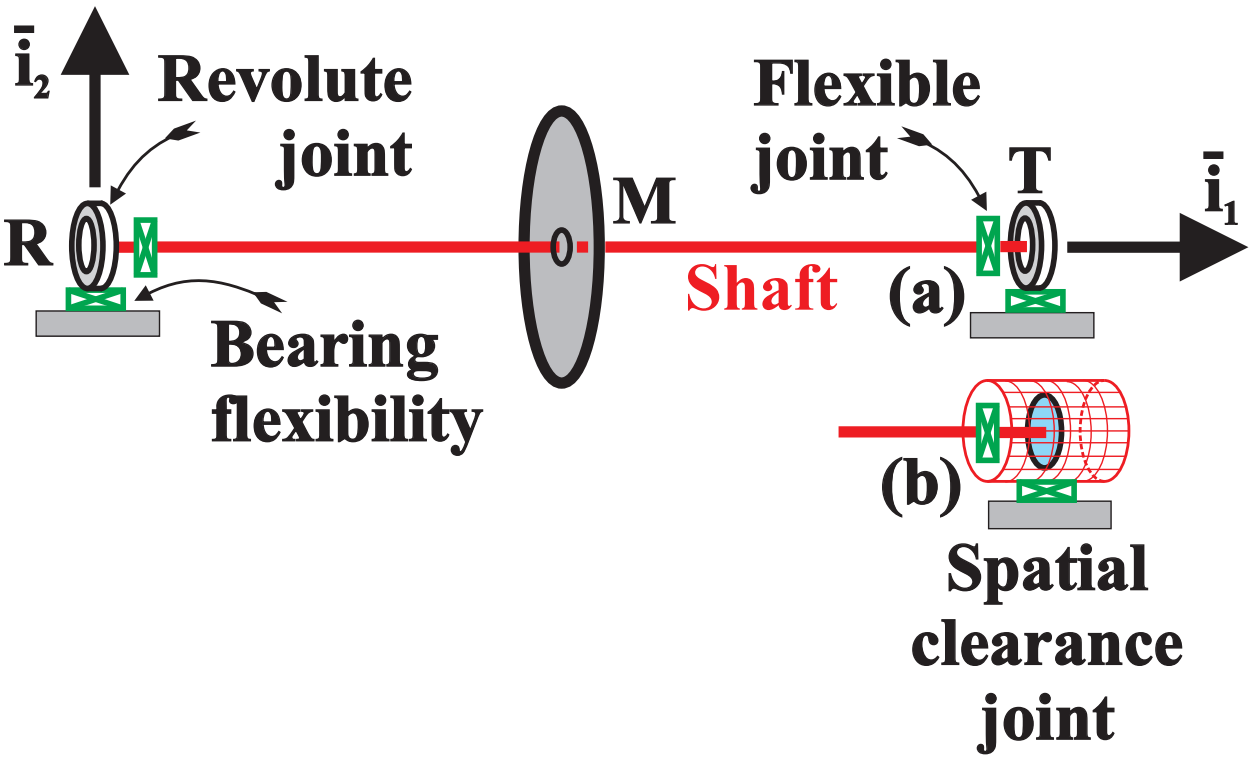

Figure 5. Flexible shaft with end flexible couplings. Configuration (a): the shaft is supported by compliant bearings. Configuration (b): the right support consists of spatial clearance joint.

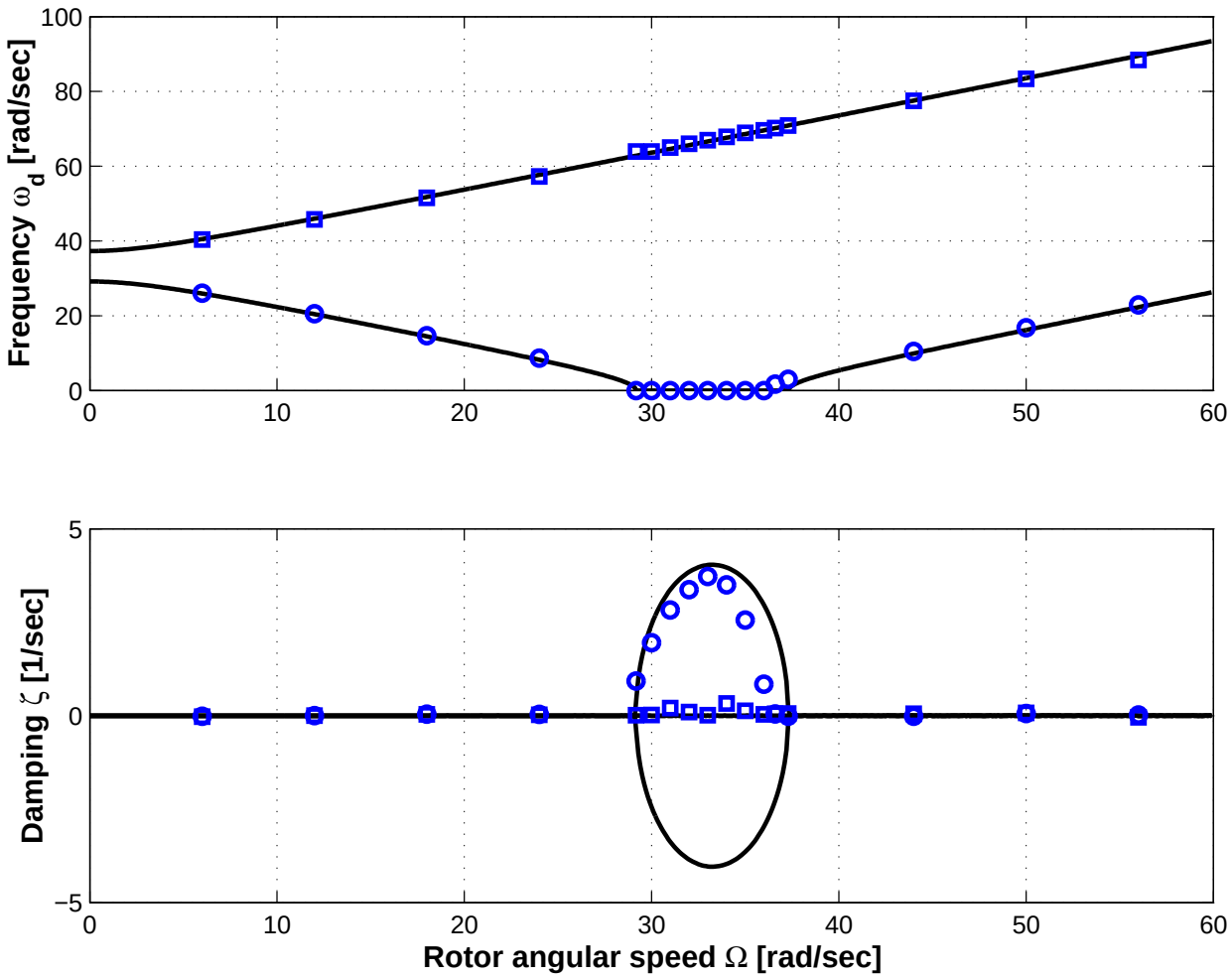

Figure 6. Frequency and damping of the two least-damped modes versus shaft angular velocity. No damping. Simplified modal solution: solid line; proposed approach: first mode, (○), second mode (□).

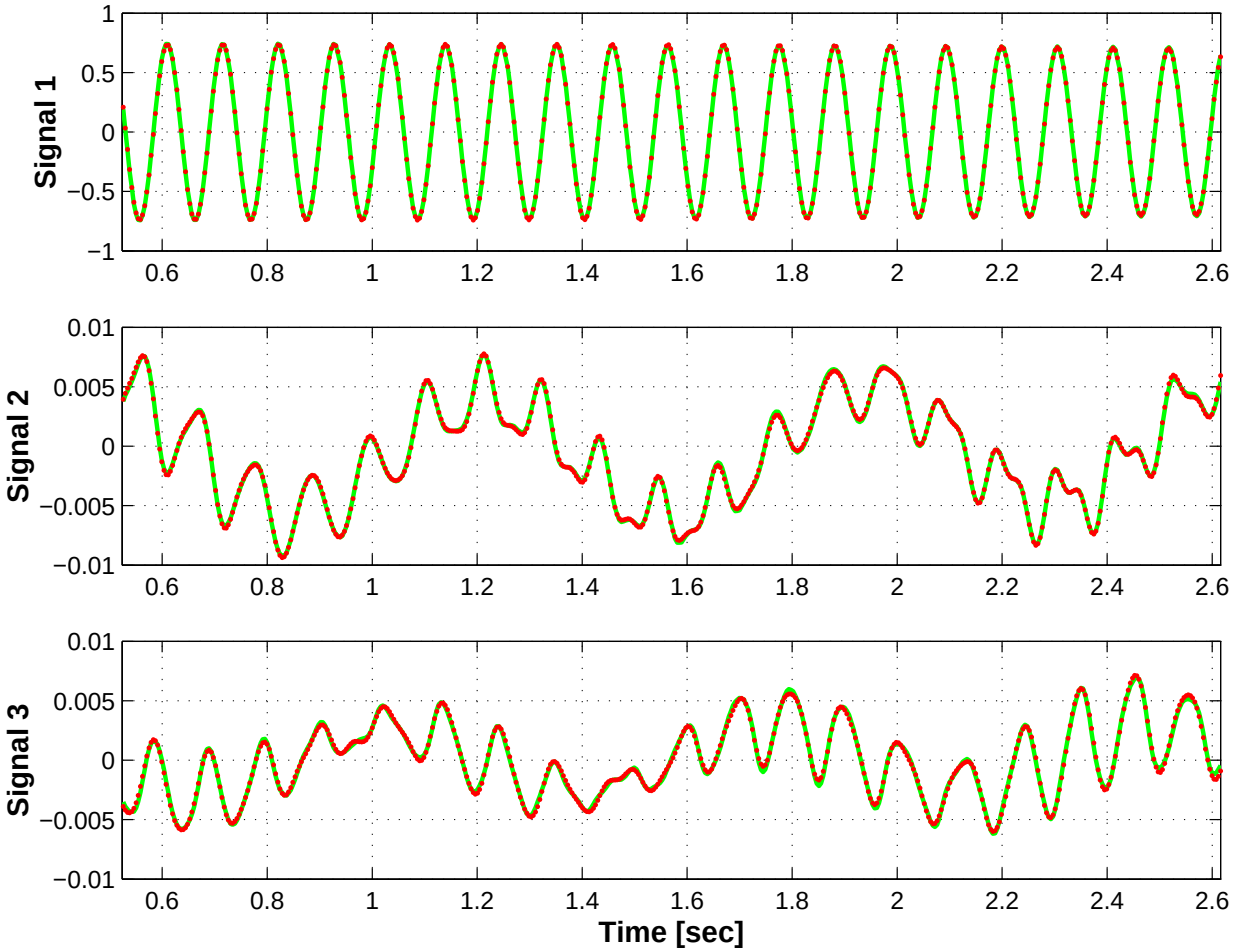

Figure 7. Original (dashed line) and reconstructed (solid line) generalized signals corresponding to the three proper orthogonal modes at $\Omega = 24$ rad/sec.

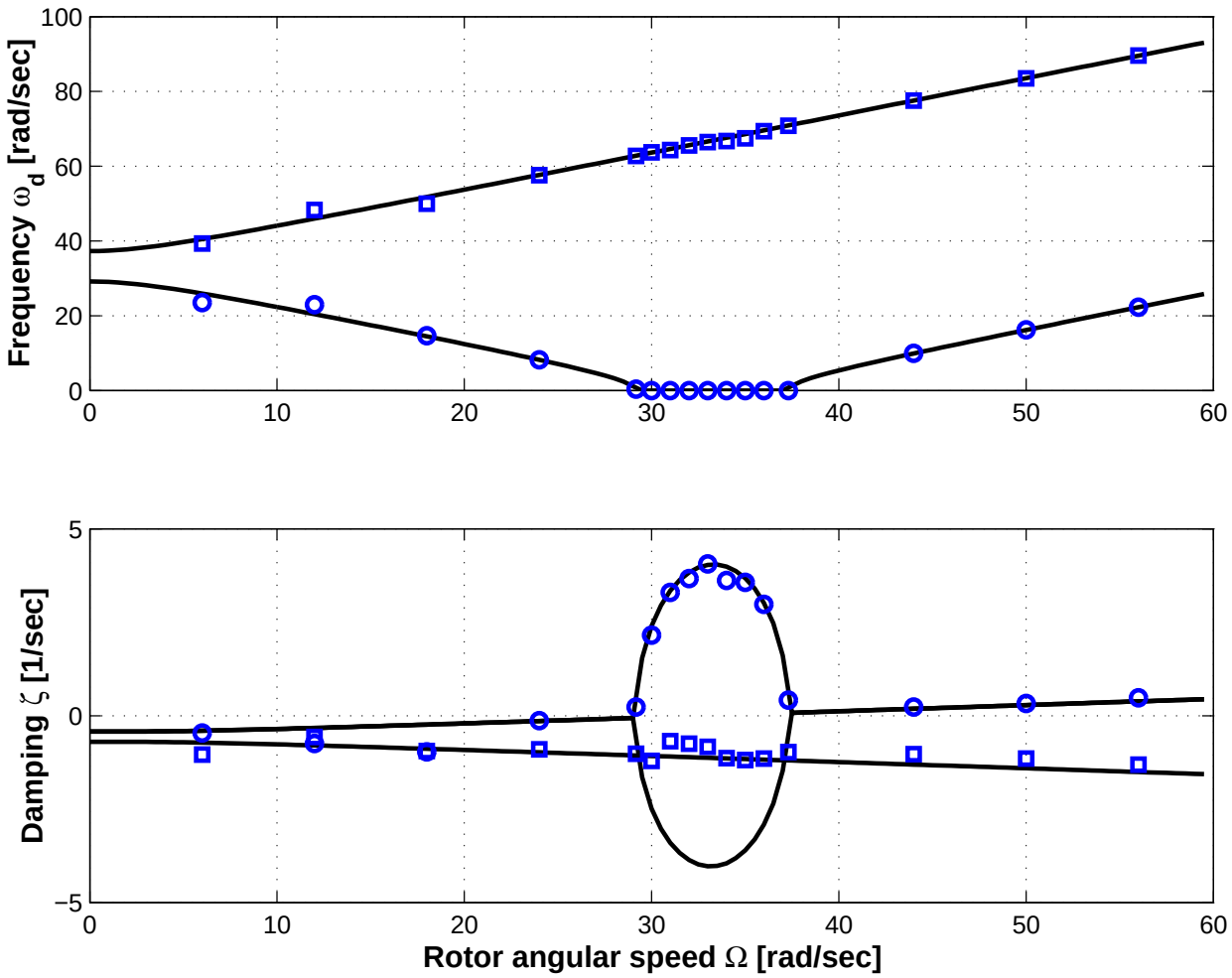

Figure 8. Frequency and damping of the two least-damped modes versus shaft angular velocity in the presence of damping. Simplified modal solution: solid line; proposed approach: first mode, (○), second mode (□).

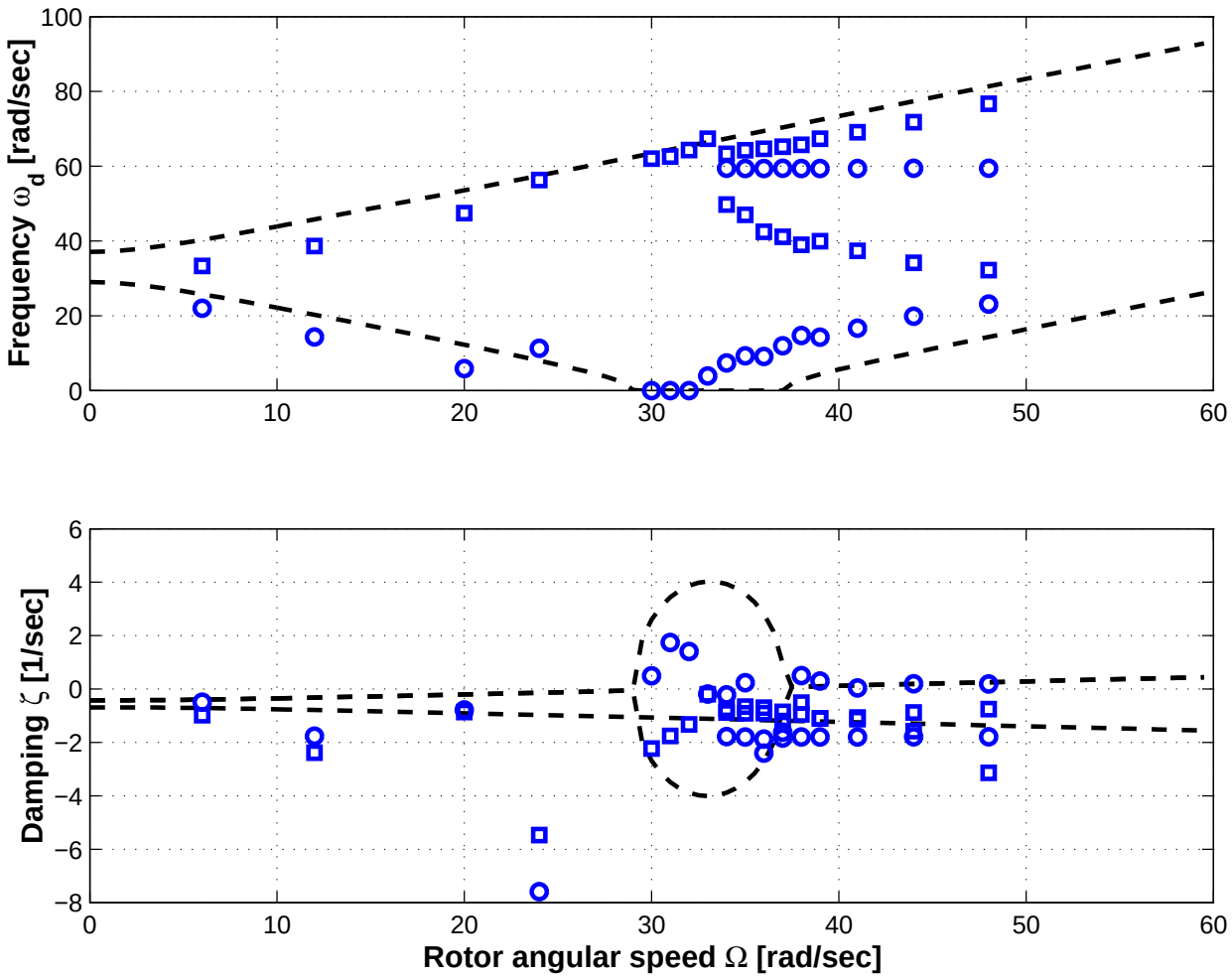

Figure 9. Frequencies and damping of the least-damped modes versus shaft angular velocity. Simplified modal solution for compliant bearings, configuration (a): dashed line. Predictions for configuration (b): symbols.

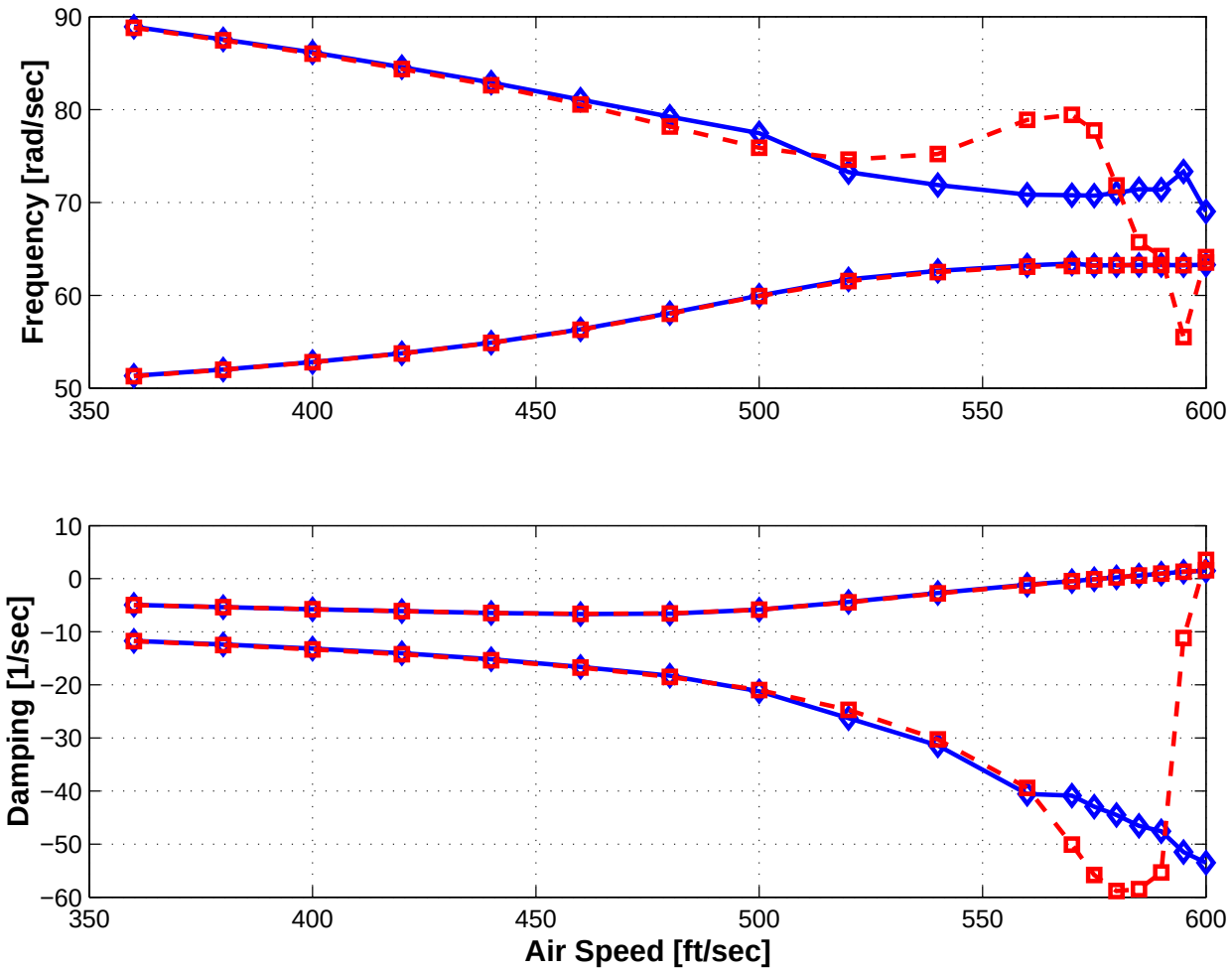

Figure 10. Frequencies and damping of the cantilevered wing. *Case 1*: dashed line (⋄): *Case 2*: solid line (□).

Appendix A The Singular Value Decomposition

The present work requires the manipulation of large data sets that are highly redundant and noisy. The main tool for extracting reliable information from these data sets is the singular value decomposition [32]. The singular value decomposition of a real rectangular matrix $S \in \mathbb{R}^{m\times n}$, $m > n$, of rank n is

$$S_{m\times n} = \left[U_{m\times n} \; \Gamma_{m\times(m-n)} \right] \begin{bmatrix} \Sigma_{n\times n} \\ 0_{(m-n)\times n} \end{bmatrix} V^T_{n\times n}, \tag{A1}$$

where $\Sigma = \mathrm{diag}(\sigma_i)$ is a unique diagonal matrix of nonnegative singular values σ_i; $[U \; \Gamma]$ an orthogonal matrix, implying $U^TU = I$, $\Gamma^T\Gamma = I$, $U^T\Gamma = 0$ and $\Gamma^TU = 0$; V an orthogonal matrix, implying $V^TV = VV^T = I$, and Γ forms the *null space* of S^T, *i.e.* $S^T\Gamma = 0$. The compact form of the singular value decomposition is $S = U\Sigma V^T$.

When dealing with highly redundant data sets, many of the singular values of S will be nearly zero. Typically, if the singular values are ordered in descending order, the following situation is encountered

$$\frac{\sigma_1}{\sigma_1} \geq \frac{\sigma_2}{\sigma_1} \geq \ldots \geq \frac{\sigma_r}{\sigma_1} \geq \frac{\sigma_{r+1}}{\sigma_1} \approx \frac{\sigma_{r+2}}{\sigma_1} \approx \frac{\sigma_n}{\sigma_1} \approx 0. \tag{A2}$$

In practice, this situation is met when $\sigma_{r+1}/\sigma_1 < \varepsilon$, $i = r+1, r+2, \ldots, n$, where ε is a small number. In effect, it follows that $\mathrm{rank}(S) = r < n$. Matrix S can now be approximated as $S \approx S_r = U_r\Sigma_rV_r^T$, where matrices U_r and V_r consist of the first r columns of U and V, respectively, and Σ_r is the $r \times r$ principal minor of Σ; it can be shown that S_r is the rank r matrix that is closest to S in the Frobenius norm. This approximation is based on the selection of the small quantity, ε; a more physically meaningful criterion to determine the rank of S is the following energy ratio criterion

$$E_r = \left(\sum_{i=1}^{r} \sigma_i \right) / \left(\sum_{i=1}^{n} \sigma_i \right), \tag{A3}$$

that indicates the amount of energy captured in the retained modes as a fraction of the total amount of energy contained in the signal.